Reaction of Ethylene with Hydroxyl Radicals: A Theoretical Study †

3 **AUTHORS**, INCLUDING:

Juan Pablo Senosiain
Laboratorios Senosiain

18 PUBLICATIONS   **595** CITATIONS

Reaction of Ethylene with Hydroxyl Radicals: A Theoretical Study[†]

Juan P. Senosiain,*,[‡] Stephen J. Klippenstein,[§] and James A. Miller*,[‡]

Combustion Research Facility, Sandia National Laboratories, MS 9055, Livermore, California 94551-0969, and Chemistry Division, Argonne National Laboratory, Argonne, Illinois 60439

Received: November 18, 2005; In Final Form: February 21, 2006

Ab initio calculations of portions of the C_2H_5O potential energy surface critical to the title reaction are presented. These calculations are based on QCISD geometries and frequencies and RQCISD(T) energies extrapolated to the complete-basis-set limit. Rate coefficients for the reaction of C_2H_4 with OH are calculated using this surface and the two transition-state model of Greenwald and co-workers [*J. Phys. Chem. A* **2005**, *109*, 6031] for the association of OH with C_2H_4. The present calculations reproduce most of the experimental data, including the temperature and pressure dependence of the rate coefficients, with only a small (0.4 kcal/mol) adjustment to the energy barrier for direct hydrogen abstraction. We confirm the importance of this channel above 800 K and find that a significant fraction of the total rate coefficient (~10%) is due to the formation of vinyl alcohol above this temperature. Calculations of the vinyl alcohol channel are consistent with the recent observation of this molecule in low-pressure flames [Taatjes, C. A.; Hansen, N.; McIlroy, A.; Miller, J. A.; Senosiain, J. P.; Klippenstein, S. J.; Qi, F.; Sheng, L.; Zhang, Y.; Cool, T. A.; Wang, J.; Westmoreland, P. R.; Law, M. E.; Kasper, T.; Kohse-Höinghaus, K. *Science* **2005**, *308*, 1887] and suggest that this reaction should be included in hydrocarbon oxidation mechanisms.

I. Introduction

The reaction of ethylene with OH is important in a number of chemical contexts. In rich flames, reaction with OH is typically the first step in the oxidation of olefins. In the troposphere, this reaction is the main mechanism responsible for the degradation of ethylene. In fact, the importance of the title reaction may extend beyond terrestrial chemistry.[1,2]

From a theoretical point of view, the reaction of ethylene with OH radicals is of great interest for several reasons. First, it is representative of a class of radical–molecule reactions that form a van der Waals complex without an energy barrier and then proceed to a molecular adduct via a pathway whose saddlepoint lies below reactants. These reactions typically show a negative temperature dependence. Second, the reaction of ethylene with OH radicals exhibits a dramatic change in activation energies around 800 K. Large deviations from Arrhenius behavior result from the switching of the dominant reaction pathway. At low temperatures the reaction proceeds entirely by addition and stabilization of the HOC_2H_4 adduct. As the temperature is increased, stabilization becomes less efficient, and at higher temperatures the isomerization and hydrogen abstraction processes overtake the addition channel. For these reasons, there have been several theoretical[3–15] studies of this reaction. Experimentally, rate coefficients have been measured down to 96 K[16] and up to shock tube[17–20] and flame[21] temperatures, but the majority of studies[22–53] have been performed around room temperature.

The role that the prereactive van der Waals complex (**C1**) has on the kinetics has been the subject of much discussion.[10,54–56]

Theoretical calculations[4] have shown that **C1** has C_{2v} symmetry, with the OH perpendicular to the C_2H_4 plane and the hydrogen pointing toward the C–C bond. Although there seems to be no saddlepoint on the potential energy surface (PES) between the reactants and **C1**, the formation of this complex is inhibited by a long-range dynamical bottleneck. At low energies (temperatures), the capture rate is controlled by the outer transition state. At higher energies the limiting bottleneck is the inner transition state between **C1** and the adduct (**1**), which involves the rotation of the OH moiety and the formation of a C–O bond. Greenwald and co-workers[56] recognized that the prereactive complex is rarely in thermal equilibrium, and thus inclusion of the prereactive complex in the analysis needs to be done at the microcanonical level. They proposed a two-transition-state model that accurately models the addition reaction. In this model, the effective flux through both transition states is given by

$$\frac{1}{N_{\text{eff}}^{\ddagger}(E)} = \frac{1}{N_{\text{inner}}^{\ddagger}(E)} + \frac{1}{N_{\text{outer}}^{\ddagger}(E)} - \frac{1}{N_{\text{max}}^{\ddagger}(E)} \qquad (1)$$

where $N_{\text{max}}^{\ddagger}(E)$ is the maximum flux through the region between the two transition states and can be reasonably assumed to be infinite compared to $N_{\text{inner}}^{\ddagger}(E)$ and $N_{\text{outer}}^{\ddagger}(E)$. In most cases, the potential in the range of the outer transition state is dominated by the dipole–quadrupole interaction, and one can use the expression derived by Georgievskii and Klippenstein[57] for obtaining $N_{\text{outer}}^{\ddagger}(E)$. Greenwald et al.[56] found that between 10 and 400 K, both transition states need to be considered in calculating the flux of the association reaction.

Of the theoretical studies on this reaction, several have investigated the kinetics[5,9,10,12,56,58] as well. Most of these rationalize the negative activation energies observed at low temperatures by directly comparing them with the negative energy barriers (i.e., below reactants) used in canonical transi-

Reaction of Ethylene with Hydroxyl Radicals

J. Phys. Chem. A, Vol. 110, No. 21, 2006 **6961**

tion-state theory calculations of the association channel. Furthermore, in some studies[58] the theoretical model chemistry is chosen on the basis of this comparison. This approach is doubly misleading because it conflates two fundamentally different quantities, and because fortuitous agreement with experiment can lead to the justification of lesser treatments of electron correlation.

Despite the importance of the title reaction in combustion chemistry, there are a number of discrepancies between experimental determinations of the rate coefficients at high temperatures.[17,18,45,46,59] For instance, there is considerable disagreement between experiments performed in a well stirred-reactor[46] and in shock tubes[17,18] between 1200 and 1300 K. Measurements at higher tempertures[59] (1850−2150 K) seem to be at odds with Arrhenius extrapolations of direct measurements done at intermediate temperatures.[45,46] In the high-temperature regime, the reaction of ethylene with OH consists almost entirely[45] of the direct abstraction channel. To the best of our knowledge, there are only two theoretical studies[12,60] that report rate coefficients of this channel, and the results differ by about 2 orders of magnitude. Thus, a theoretical reexamination of this reaction at high temperatures is warranted.

The objective of this study is to bridge the existing data from low- and high-temperature measurements using a sound theoretical model. We present high-level ab initio calculations of isomers and (low energy) saddlepoints on the C_2H_5O PES pertinent to the reaction of ethylene with OH radicals. Energy levels derived from this surface and from the model of Greenwald and co-workers[56] are used in conjunction with a multichannel-master equation model to compute rate coefficients over a broad range of temperatures and pressures. In section II we describe the details of the ab initio calculations and the computation of the rate coefficients, and these are discussed in section III. Finally, to facilitate the use of the present results in chemical kinetics models, we provide empirical fits of the calculated rate coefficients in the last section.

II. Computational Details

A. Quantum Chemistry. The geometries and vibrational frequencies of stable species and first-order saddlepoints were optimized using Pople's split-valence 6-311++G(d,p) Gaussian basis set and two different treatments of electron correlation. The first method consisted of spin-unrestricted hybrid density functional theory with the B3LYP functional.[61,62] The second set of geometry optimizations was done using the same basis set and the spin-unrestricted, quadratic configuration-interaction method, with singles and doubles excitations, UQCISD.

Because energy barriers affect the calculated rate coefficients exponentially, we refined the energies by performing single-point energy calculations on the UB3LYP and UQCISD geometries using the RQCISD(T) method, together with Dunning's correlation-consistent basis sets. The energies were extrapolated to the infinite-basis-set limit with the asymptotic form suggested by Martin[63] and by Dixon and Feller,[64]

$$E_\infty = E_{l_{max}} - B/(l_{max} + 1)^4 \qquad (2)$$

where l_{max} is the maximum component of angular momentum in the cc-pVnZ basis set, and E_∞ the infinite basis-set energy. In this case triple and quadruple-ζ basis sets were used, i.e., $l_{max} = \{3, 4\}$. Henceforth, we shall denote properties obtained at the RQCISD(T)/cc-pV∞Z level and UB3LYP/6-311++G-(d,p) and UQCISD/6-311++G(d,p) geometries and vibrational frequencies simply as RQCIT//DFT and RQCIT//QCI, respec-

tively. The related RCCSD(T) method has been shown[65] to achieve "chemical accuracy", even in situations where spin contamination would normally be a problem. However, our own unpublished calculations[66] show that the RQCISD(T) method performs slightly better than the popular RCCSD(T) in the calculation of a series of well-known adiabatic energy barriers.[67]

The RQCISD(T) calculations were performed using the Molpro[68] electronic structure package, and Gaussian98[69] was used for all other quantum chemistry calculations, including geometry optimizations, vibrational frequencies and intrinsic reaction coordinates (IRC). All calculations were performed in a 16-processor cluster running Linux.

B. Calculation of Rate Coefficients. Microcanonical rate coefficients as a function of total energy and total angular momentum were calculated using RRKM theory. Energy levels were computed within the rigid rotor and harmonic oscillator approximations using optimized geometries and vibrational frequencies from the UQCISD/6-311++G(d,p) calculations. Densities of states and cumulative numbers of states were obtained with the exact counting method. Internal rotors were accounted for within the Pitzer−Gwinn approximation[70] using Fourier fits to the UB3LYP rotation potentials, as described elsewhere.[71] These potentials are provided in the Supporting Information. Coupling between internal rotations in species with more than one torsional mode was neglected. Asymmetric Eckart barriers were employed to compute the effects of (1-d) tunneling and nonclassical reflection. For the addition reaction, we used the "effective" number of states obtained from the two-transition-state model of Greenwald and co-workers.[56] All other reaction channels were computed using energies calculated with the RQCIT//QCI theoretical model chemistry discussed in the previous section.

The rate coefficients as a function of pressure and temperature were computed by solving the total-energy resolved (i.e., 1-d) master equation (ME) for the three well system,

$$\frac{dn_i(E)}{dt} = Z \int_{E_{0_i}}^{\infty} P(E \leftarrow E') \, n_i(E') \, dE' - Zn_i(E) -$$
$$\sum_{j \neq i}^{3} k_{ji}(E) \, n_i(E) + \sum_{j \neq i}^{3} k_{ij}(E) \, n_j(E) -$$
$$\sum_{\alpha} k_{P_\alpha i}(E) \, n_i(E) + n_R K_{R_i}^{eq} k_{R_i}(E) \frac{\rho_i(E) e^{-\beta E}}{Q_i(T)} -$$
$$k_{R_i}(E) \, n_i(E) \qquad (3)$$

where $i = \{1, 2, 3\}$ corresponds to $HOCH_2CH_2$, OCH_2CH_3 and $HOCHCH_3$, respectively, **R** corresponds to the reactants (OH + C_2H_4) and P_α to bimolecular products, **P1** = H_2CO + CH_3, **P2** = H + $OCHCH_3$, **P3** = H_2O + $CHCH_2$ and **P4** = H + $HOCHCH_2$. In eq 3, $n_i(E)$ is the population of complex i at energy E, E_{0_i} is the ground-state energy of complex i, Z is the collision number per unit time and $K_{R_i}^{eq}$ is the pseudo-first order equilibrium constant between **R** and complex i. The term involving $k_{ji}(E)$ represents the rate of isomerization from i to j, where i, j are the stable isomers.

Collision rates were calculated using the Lennard-Jones potential parameters of ethanol[72] to represent the complexes. $P(E \leftarrow E')$ is the probability that a complex with an energy between E' and $E' + dE'$ will be transferred by a collision to a state with an energy between E and $E + dE$. The rates of collisional energy transfer (CET) for deactivating collisions were modeled using the "single exponential down" expression:

$$P(E \leftarrow E') \propto \exp\left(-\frac{E' - E}{\langle \Delta E_d \rangle}\right) \qquad E' > E \qquad (4)$$

where $\langle \Delta E_d \rangle$ is an energy transfer parameter that depends on the nature of the collider gas, in this case N_2. We employ a value of $\langle \Delta E_d \rangle = 200$ cm$^{-1}(T/298$ K)$^{0.85}$ for all complexes. This value was used by Greenwald et al.[56] to fit experimental falloff curves[16,24,30,37,39,50,52,53] at several temperatures. CET rates for activating collisions were obtained from detailed balance. Dissociation to bimolecular products was treated irreversibly. Rate coefficients were extracted from the solution eigenpairs following procedures described elsewhere.[73-75] All rate coefficients were calculated with the VARIFLEX code.[76]

For the special case of reactions at the collisionless limit ($Z \rightarrow 0$), the two-dimensional master equation, i.e., resolved in terms of E (total energy) and J (total angular momentum quantum number), can be solved to obtain the phenomenological rate coefficients.[77,78] Rotational effects are generally greatest in the absence of collisions, so comparison of the 1-d and 2-d rate coefficients in the collisionless limit should provide an upper bound for the magnitude of these effects.

Variational effects in the hydrogen abstraction channel were accounted for by calculating the (*E*- and *J*-resolved) rate coefficients with a fixed and a variable transition state, using the RQCIT//DFT theoretical model chemistry. The final rate coefficients were obtained by multiplying the conventional transition-state theory values at the higher level of theory (i.e., RQCIT//QCI) by the variational corrections at each temperature.

Spin−orbit interactions in the OH radical (at rest) cause a splitting of 126 cm^{-1} between the $^2\Pi_{3/2}$ and $^2\Pi_{1/2}$ ground-state levels.[79] This splitting increases with the total angular momentum quantum number. In contrast, spin−orbit splitting in the transition state is expected to be negligible because the coupling with the molecule's rotational axes is very weak. We incorporated spin uncoupling effects into the analysis by correcting the partition function of the reactants. Additional corrections were included to account for the fact that the Variflex code restricts the total angular momentum quantum number (J) to integer values when half-integer values are needed in the case of open-shell species. The combined correction factor for these two effects is 0.88 at room temperature and approaches unity as the temperature increases.

III. Results and Discussion

A. C2H5O Potential Energy Surface. Despite the abundance of ab initio studies[3-9,11-15] in the literature involving the C2H5O PES, we recomputed portions of this surface for several reasons. Only two of these studies include all the (low-energy) channels relevant to the reaction of ethylene with OH, and the treatment of electron correlation and basis sets can be improved. Quantum chemical methods used in computing reaction energy barriers in this work do not contain empirical "high-level" corrections. In addition, the use of the UQCISD method for the computation of geometries and frequencies, although computationally expensive, should provide improved values for the calculation of rate coefficients.

Stationary points of the PES for the reaction of OH with ethylene are shown schematically in Figure 1. Briefly, the reactants form a hydrogen-bonded complex (**C1**) before they add to form 2-hydroxyethyl radical (**1**). Alternatively, the reactants can undergo direct hydrogen abstraction to form water and vinyl radicals (**P3**). **1** can undergo a [1,3] or [1,2]-hydrogen shift to ethoxy radical (**2**) or 1-hydroxyethyl radical (**3**), respectively, or it can decompose to vinyl alcohol and H atoms
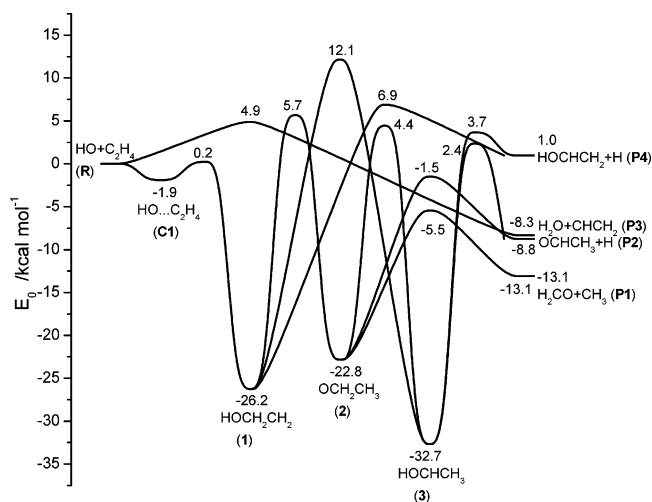

Figure 1. Simplified C2H5O potential energy surface using the RQCIT/QCI theoretical model chemistry (see text for details).

(**P4**). In turn, **2** can isomerize to **3** or decompose to formaldehyde and methyl (**P1**) or acetaldehyde and H atoms (**P2**); **3** can decompose to **P2** or **P4**.

Some of the structures in Figure 1 have more than one conformation. In this case we have used the energy of the most stable conformation, with the implicit assumption that conformational rearrangements are rapid relative to chemical reactions and are thus best treated as internal rotations. In the case of the ethoxy radical there is an excited electronic state only ≈ 0.5 kcal/mol higher than the ground state $\tilde{X}(A'')$. Although some reactions (e.g., **2 $\leftrightarrow$ 3**) correlate diabatically with the $\tilde{A}(A')$ state of **2**, we have assumed that internal conversion between these states is rapid and used the energy corresponding to the ground state.

Calculated energy barriers are given in Table 1, alongside others from recent theoretical studies. Our RQCIT//QCI barriers agree within 1 kcal/mol with the values reported by Zhu and Lin,[58] Piqueras et al.[11] and Sekušak[6] for the addition channel, as well as with those of Zhang et al.[15] for decomposition of the ethoxy radical. However, our RQCIT//QCI barriers differ from those reported by Liu et al.[12] by as much as 2.7 kcal/mol in some cases. Interestingly, agreement between our RQCIT//DFT barriers and those of Liu et al. is worse, despite both of these being QCISD(T) single-point energies based on B3LYP geometries. This gives an indication of the importance of the basis set extrapolation in calculating post-Hartree−Fock energy barriers. The barrier reported by Hippler and Viskolcz[60] for TS-(**3↔P2**) seems too low and probably corresponds to a van der Waals complex.

The rotational constants of the structures optimized with the UQCISD and UB3LYP methods are shown in Table 2, along with the external and total symmetry numbers and numbers of optical isomers used in the transition-state theory calculations. In general, the geometries of structures optimized with both methods are similar, but transition-state structures obtained with the UQCISD method have somewhat shorter bond lengths, with the largest differences occurring in the dissociation transition states. For example, the H−X bond lengths of TS(**2↔P2**), TS-(**2↔P1**) and TS(**3↔P2**) are shorter by 0.11, 0.09, and 0.08 Å, respectively, when optimized with UQCISD instead of UB3LYP.

Previous studies[5,11,58] have found several structures on the C2H5O PES to be quite sensitive to the treatment of electron correlation. For example, we did not find a saddlepoint for the dissociation of the 1-hydroxyethyl radical into vinyl alcohol +

Reaction of Ethylene with Hydroxyl Radicals

J. Phys. Chem. A, Vol. 110, No. 21, 2006 **6963**

TABLE 1: Comparison of Calculated Energy Barriers[a] with Recent Theoretical Studies

	this work[b]	ref 58[c]	ref 15[d]	ref 12[e]	ref 11[f]	ref 60[g]	ref 10[h]	ref 8[i]	ref 9[j]	ref 6[k]
1 → 2	31.9	34.0		31.2		32.3		29.1	29.8	
1 → 3	38.4	37.7		39.6		39.4				
1 → P4	33.1	31.9		31.5		32.8			34.2	
2 → 1	28.5	25.1	29.5	31.2					23.5	
2 → 3	27.2		26.9	30.0		27.3		26.2		
2 → P1	17.4	13.8		17.7		16.9		20.8	13.4	
2 → P2	21.3			20.6		20.0		23.1	17.6	
3 → P2	35.0			32.6		23.1				
3 → P4	36.3					38.0				
R → 1		−0.8		−2.2	−0.3		−0.5			−0.69
C1 → 1	2.1	1.1		0.1	2.24					1.35
R → P3	4.9	5.9		6.6		8.4				

[a] Units are kcal/mol. [b] RQCISD(T)/cc-pV∞Z//UQCISD/6-311++G(d,p). [c] PMP2/aug-cc-pVQZ//MP2/cc-pVTZ. [d] QCISD(T)/aug-cc-pVTZ//MPW1K/6-31+G(d,p). [e] QCISD(T)/ 6-311G(2df,p)//B3LYP/6-311G(d,p). [f] CBS-QB3. [g] QCISD(T)/6-311+G(3df,2p)//MP2/6-311G**. [h] PMP2/aug-cc-pVTZ//MP2/6-311G**. [i] MP2/6-311+G**//MP2/6-31G*. [j] CBS-Q. [k] MP2/aug-cc-pVTZ//MP2(full)/6-311+G(2d,p).

TABLE 2: Calculated Rovibrational Properties of Isomers, Bimolecular Products and Saddlepoints

	symm	species	B_{rot}[a]			B_{rot}[b]			σ_{ext}[c]	σ_{tot}[d]	m[e]
R	^1A_g	C_2H_4	4.87	0.99	0.83	4.91	1.01	0.84	4	4	1
	$^2\Pi$	OH	18.85			18.66			1	1	1
C1	$^2B_1$	OH..C_2H_4	0.82	0.13	0.12	0.83	0.14	0.12	2	2	1
1	$^2A'$	$HOCH_2CH_2$	1.27	0.33	0.28	1.28	0.33	0.28	1	2	1
2'	$^2A'$	OCH_2CH_3	1.16	0.34	0.30	1.17	0.34	0.30	1	3	1
2	$^2A''$	OCH_2CH_3	1.30	0.32	0.28	1.33	0.32	0.28	1	3	1
3	^2A	$HOCHCH_3$	1.45	0.31	0.28	1.48	0.31	0.27	1	3	1
	$^1A_1$	H_2CO	9.49	1.29	1.14	9.46	1.30	1.14	2	2	1
	$^2A_2''$	CH_3	9.50	9.50	4.75	9.55	9.55	4.77	6	6	1
	$^1A'$	CH_3CHO	1.89	0.34	0.30	1.91	0.34	0.30	1	3	1
	$^1A_1$	H_2O	26.83	14.73	9.51	27.52	14.34	9.43	2	2	1
	^2A	$CHCH_2$	7.71	1.07	0.94	7.92	1.09	0.96	1	1	1
	$^1A'$	CH_2CHOH	2.00	0.35	0.30	2.02	0.35	0.30	1	1	1
	^2A	**1 ↔ 2**	0.94	0.44	0.34	0.94	0.44	0.34	1	1	1
	^2A	**1 ↔ 3**	1.54	0.32	0.28	1.56	0.32	0.28	1	1	2
	^2A	**1 ↔ P4**	1.31	0.33	0.29	1.31	0.33	0.29	1	1	2
	^2A	**2 ↔ 3**	1.47	0.31	0.28	1.49	0.31	0.28	1	3	2
	^2A	**2 ↔ P1**	1.09	0.26	0.23	1.11	0.24	0.22	1	3	1
	^2A	**2 ↔ P2**	1.31	0.32	0.29	1.28	0.32	0.29	1	3	2
	^2A	**3 ↔ P2**	1.44	0.32	0.28	1.47	0.31	0.28	1	3	1
	^2A	**3 ↔ P4**	1.36	0.31	0.28				1	1	2
	^2A	**R ↔ 1**	0.93	0.26	0.22	0.87	0.15	0.14	1	1	1
	^2A	**R ↔ P3**	1.41	0.18	0.16	1.45	0.17	0.16	1	1	1

[a] Rotational constants (cm^{-1}), calculated at the UQCISD/6-311++G(d,p) level. [b] Calculated at the UB3LYP/6-311++G(d,p) level. [c] Symmetry number of external rotation. [d] Total symmetry number, including internal rotations. [e] Number of optical isomers, adjusted for internal rotations.

H, i.e., TS(**3→P4**), at the UB3LYP level. It is not clear whether this saddlepoint exists on the UB3LYP surface, because the reverse barrier for this reaction is small (~1.5 kcal/mol without ZPE), and DFT methods are prone to underestimating energy barriers.[67] Similarly, the structure of the **C1** complex obtained in the present UB3LYP calculations and in previous theoretical studies[4,56,58] has C_{2v} symmetry, yet the UQCISD geometry has no symmetry, with the OH almost 20° off the C_2 axis.

Vibrational frequencies obtained with the two methods are shown in Tables 3 and 4. It is a common practice to scale ab initio vibrational frequencies by an empirical correction factor.[80,81] The effect of scaling the computed frequencies is small and so can probably be neglected. We have chosen not to do so, because the low frequencies corresponding to the transitional modes of transition states scale quite differently from the others. However, differences in the frequencies calculated with the two methods have important effects on the resulting rate coefficients. This is particularly true for the transitional modes, even at temperatures relevant to combustion. For instance, in the hydrogen abstraction channel, the torsional frequency calculated with the UQCISD method (95 cm^{-1}) is smaller than the UB3LYP value (121 cm^{-1}). If treated harmonically, the dif-

ference in this degree of freedom alone corresponds to an enhancement of the rate coefficient of about 27% (above 250 K).

The width of the energy barrier, in this case obtained from the imaginary frequency of the saddlepoint, has a strong effect on the Eckart transmission coefficient. The calculated imaginary frequencies of transition states are very sensitive to the level of theory employed. For example, the imaginary frequencies calculated with the UB3LYP and UQCISD methods are 1127i and 1892i cm^{-1}, respectively, for the H abstraction channel, and 1973i and 2226i cm^{-1} for the **1 ↔ 2** isomerization. At very low temperatures and pressures (e.g., conditions relevant to interstellar chemistry), rate coefficients depend critically on tunneling. However, the association reaction dominates below 300 K, even at pressures as low as 0.01 atm N_2. Because the energy barrier of the addition reaction is broad and below the energy of the reactants, tunneling in this channel is unimportant.

The calculated zero-point energies (ZPE) and the ground-state energies (including ZPE) are tabulated in Table 5. At lower temperatures, inaccuracies in the frequencies affect the calculated rate coefficients mostly through the ZPE's rather than through the vibrational entropy. In most cases, the RQCISD-(T) energies calculated at UQCISD and UB3LYP optimized

TABLE 3: Vibrational Frequencies Calculated at the UQCISD/6-311++G(d,p) Level

species	frequencies^a (cm^{-1})																	
C$_2$H$_4$	802	832	957	1041	1242	1380	1487	1685	3150	3169	3231	3258						
OH	3774																	
C1	63	85	95	241	298	833	889	975	1052	1244	1380	1488	1682	3149	3167	3232	3258	3757
1	**196**	**369**	433	535	845	977	1120	1144	1204	1389	1432	1482	1516	3024	3056	3160	3271	3893
2′	**251**	395	739	918	994	998	1151	1305	1342	1416	1499	1518	1560	3015	3067	3074	3151	3160
2	**310i**	250	434	895	907	1096	1122	1384	1397	1418	1446	1514	1525	2971	3028	3055	3131	3144
3	**222**	**395**	417	654	928	1046	1082	1217	1323	1421	1468	1493	1506	2995	3063	3132	3210	3887
H$_2$CO	1204	1280	1558	1800	2954	3017												
CH$_3$	464	1435	1435	3126	3308	3308												
CH$_3$CHO	**142**	511	785	905	1143	1146	1405	1445	1488	1492	1812	2940	3052	3121	3170			
H$_2$O	1654	3889	3992															
CHCH$_2$	738	801	916	1080	1409	1634	3094	3198	3261									
CH$_2$CHOH	**391**	490	692	743	964	978	1138	1332	1371	1465	1714	3169	3227	3274	3884			
1 ↔ 2	2226i	364	719	829	954	1002	1100	1107	1169	1220	1327	1457	1547	1950	3095	3129	3158	3242
1 ↔ 3	2104i	356	**415**	443	732	819	966	1111	1199	1288	1321	1414	1468	2180	3145	3171	3297	3902
1 ↔ P4	1020i	**392**	437	470	505	672	803	960	1038	1132	1315	1360	1465	1622	3172	3230	3279	3889
2 ↔ 3	2130i	**200**	429	630	906	925	1090	1135	1198	1384	1434	1494	1505	2435	3036	3109	3112	3149
2 ↔ P1	499i	**153**	284	532	593	681	935	1116	1260	1440	1455	1483	1621	2964	3027	3104	3264	3278
2 ↔ P2	1119i	**194**	452	511	534	846	931	1121	1147	1400	1426	1492	1495	1659	2953	3055	3131	3167
3 ↔ P2	1762i	**85**	**229**	489	639	762	946	1092	1139	1393	1423	1482	1497	1632	3029	3039	3116	3162
3 ↔ P4	717i	**246**	339	440	491	754	906	953	988	1139	1329	1367	1465	1665	3172	3232	3278	3879
R ↔ 1	366i	**140**	222	369	718	830	879	986	1013	1245	1324	1486	1610	3161	3186	3252	3284	3792
R ↔ P3	1892i	**95**	152	300	568	781	824	858	954	1131	1260	1301	1423	1673	3141	3217	3237	3820

^{a} Frequencies in boldface were treated as internal rotations.

TABLE 4: Vibrational Frequencies Calculated at the UB3LYP/6-311++G(d,p) Level

species	frequencies^a (cm^{-1})																	
C$_2$H$_4$	833	972	975	1057	1238	1377	1471	1682	3126	3140	3199	3227						
OH	3707																	
C1	72	98	104	270	354	836	985	994	1067	1239	1377	1474	1678	3124	3137	3197	3225	3623
1	**180**	**345**	427	558	824	949	1077	1119	1178	1354	1395	1451	1482	2975	2996	3135	3244	3818
2′	**250**	384	625	897	923	969	1124	1253	1298	1385	1471	1498	1534	2949	2988	3044	3121	3134
2	**132**	268	434	864	886	1067	1096	1236	1334	1386	1408	1484	1494	2886	2887	3030	3095	3107
3	**202**	**355**	411	578	913	1016	1059	1196	1293	1399	1433	1468	1483	2930	3006	3093	3192	3817
H$_2$CO	1202	1260	1530	1814	2887	2945												
CH$_3$	537	1402	1402	3103	3283	3283												
CH$_3$CHO	**152**	510	776	886	1128	1133	1378	1420	1460	1469	1808	2871	3021	3075	3136			
H$_2$O	1602	3818	3924															
CHCH$_2$	707	817	923	1042	1390	1644	3038	3137	3240									
CH$_2$CHOH	**454**	490	708	825	957	991	1119	1315	1349	1445	1693	3140	3191	3239	3807			
1 ↔ 2	1973i	386	715	821	918	977	1076	1081	1143	1208	1298	1430	1523	1917	3056	3095	3115	3208
1 ↔ 3	1926i	355	**410**	439	711	794	943	1083	1165	1253	1295	1392	1438	2140	3101	3140	3263	3827
1 ↔ P4	727i	**389**	434	442	496	674	815	954	1018	1115	1308	1335	1443	1606	3146	3197	3248	3812
2 ↔ 3	1981i	**190**	429	608	875	901	1061	1113	1172	1358	1404	1470	1480	2374	2995	3058	3070	3112
2 ↔ P1	328i	**128**	268	501	539	590	896	1102	1239	1409	1424	1483	1627	2896	2949	3091	3256	3269
2 ↔ P2	792i	**172**	383	442	503	807	902	1097	1126	1376	1399	1463	1474	1687	2866	3022	3089	3134
3 ↔ P2	1166i	**98**	141	486	566	756	906	1088	1126	1375	1401	1455	1470	1646	2954	3003	3067	3130
3 ↔ P4																		
R ↔ 1	145i	**50**	110	181	209	835	980	991	1060	1238	1375	1472	1673	3124	3137	3198	3226	3695
R ↔ P3	1127i	**121**	163	307	603	791	837	884	962	1127	1224	1268	1405	1662	3102	3176	3193	3764

^{a} Frequencies in boldface were treated as internal rotations.

geometries differ by less than 0.5 kcal/mol, but the differences can be as large as 1.4 kcal/mol, as in the case of the saddlepoints corresponding to **2 ↔ P2** and **3 ↔ P2**. The difference is reduced if IRCmax[92] values are used instead of single-point energy barriers. In general, the variations due to the ZPE are smaller than those due to the total energies.

The Q1 diagnostic (also called T1 diagnostic in some electronic structure codes) of Lee et al.[82,83] for these structures is also shown in Table 5. It gives an indication of the multireference character of a wave function. In most cases, the value of Q1 is quite small (≤0.02), indicating that the single-reference method gives an appropriate description of the wave function. The saddlepoints corresponding to TS(**R↔1**) and TS-(**3↔P2**) have a somewhat large (≥0.03) Q1 diagnostic, suggesting that multireference calculations might yield better energies. However, the former TS was not used in the kinetics (we used the model of ref 56) and the latter plays a relatively

minor role in the overall rate coefficients. Furthermore, on the basis of our experience with the analogous C$_2$H$_3$O system,[84] we expect the multireference configuration-interaction method with Davidson correction, MRCI+Q, to give energy barriers that agree with the RQCIT barriers within the estimated uncertainty of these methods (≈2 kcal/mol).

B. Rate Coefficients. The eigenvalues of the master equation corresponding to chemical processes are plotted in Figure 2 as a function of temperature. The quasi-continuum of eigenvalues corresponding to internal energy relaxation (IERE) is shown in Figure 2 with gray shading. At low temperatures the smallest (i.e., least negative) eigenvalues correspond to the dissociations of **2** and **3** to bimolecular products. The eigenvalues corresponding to the stabilization of complex **2** and the dissociation of reactants to products display an "avoided crossing" around 700 K. At about 1200 K, the eigenpair corresponding to the dissociation of the ethoxy radical enters the IERE region,

Reaction of Ethylene with Hydroxyl Radicals

J. Phys. Chem. A, Vol. 110, No. 21, 2006 **6965**

TABLE 5: Calculated Energies, Q1 Diagnostic and Zero-Point Energies of Isomers and Bimolecular Products

	symm	species	energy (kcal/mol)			Q1 diag^d	ZPE (kcal/mol)	
			QCI^a	RQCIT//QCI^b	RQCIT//DFT^c		QCI^a	DFT^e
R	^1A_g	C_2H_4	0.0	0.0	0.0	0.011	31.8	31.9
	$^2\Pi$	OH				0.007	5.4	5.3
C1	$^2B_1$	OH..C_2H_4	−1.5	−1.9	−1.7	0.010	38.2	38.4
1	$^2A'$	$HOCH_2CH_2$	−23.1	−26.2	−27.0	0.011	41.5	40.8
2	$^2A''$	OCH_2CH_3	−22.2	−22.8	−22.1	0.019	41.1	41.3
3	^2A	$HOCHCH_3$	−29.2	−32.7	−33.6	0.016	42.1	41.2
P1	$^1A'$	H_2CO	−12.8	−13.1	−13.4	0.016	16.9	16.6
	$^2A_2''$	CH_3				0.021	18.7	18.6
P2	$^1A'$	CH_3CHO	−6.5	−8.8	−9.3	0.015	35.1	34.6
	$^2S_{1/2}$	H				0.000		
P3	$^1A_1$	H_2O	−5.2	−8.3	−8.8	0.007	13.4	13.6
	^2A	$CHCH_2$				0.017	23.1	22.8
P4	^1A	CH_2CHOH	6.0	1.0	0.8	0.013	35.5	35.3
	$^2S_{1/2}$	H				0.000		
	^2A	**1 ↔ 2**	11.2	5.7	5.1	0.021	39.1	38.5
	^2A	**1 ↔ 3**	18.2	12.1	11.5	0.012	38.9	38.2
	^2A	**1 ↔ P4**	13.2	6.9	6.1	0.019	36.8	36.4
	^2A	**2 ↔ 3**	9.6	4.4	3.7	0.014	38.8	38.1
	^2A	**2 ↔ P1**	−2.5	−5.5	−6.5	0.023	38.9	38.1
	^2A	**2 ↔ P2**	2.4	−1.5	−2.9	0.022	36.5	35.7
	^2A	**3 ↔ P2**	6.8	2.4	1.0	0.032	36.0	35.3
	^2A	**3 ↔ P4**	10.0	3.7	4.0	0.018	36.7	36.1
	^2A	**R ↔ 1**	3.0	0.2	−0.5	0.030	39.3	38.0
	^2A	**R ↔ P3**	9.1	4.9	5.0	0.028	35.4	35.1

^{a} UQCISD/6-311++G(d,p). ^{b} RQCISD(T)/cc-pV∞Z//UQCISD/6-311++G(d,p). See text for details. ^{c} RQCISD(T)/cc-pV∞Z//UB3LYP/6-311++G(d,p). See text for details. ^{d} Q1 diagnostic. ^{e} UB3LYP/6-311++G(d,p).
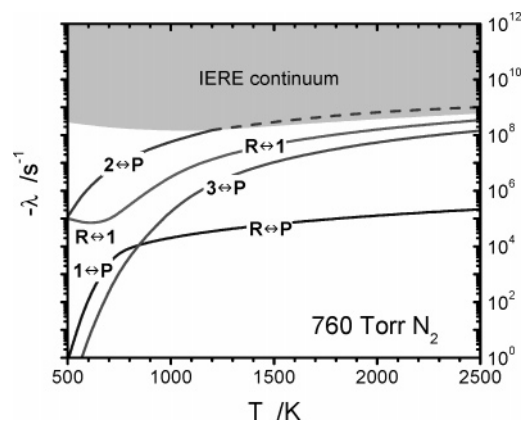
Figure 2. Chemically significant eigenvalues of the master equation for 760 Torr of N_2 collider gas. Shaded region corresponds to the quasicontiuum of internal energy relaxation eigenvalues.
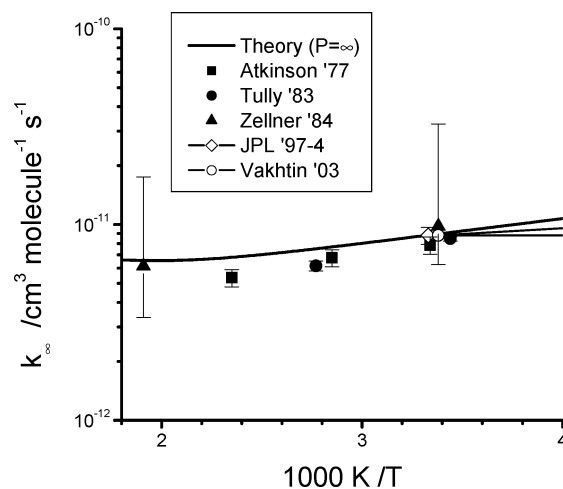

Figure 3. Arrhenius plot for the total rate coefficient at the high-pressure limit. Experimental data reported to be at the high-pressure limit from Vakhtin et al.,[16] Demore et al.,[85] Zellner and Lorenz,[41] Tully[37] and Atkinson et al.[32]

indicating that this reaction occurs on the same time scale as that of internal energy relaxation. The correct phenomenological rate coefficients can be obtained by the "initial rate" method of Klippenstein and Miller by truncating the summation in eq 30 of ref 74.

At high pressures most of the rate coefficient is due to the stabilization of C_2H_5O isomers. Our calculations indicate that, even at 500 K (at atmospheric pressure), 77% of the total rate coefficient proceeds through the electrophilic addition reaction. The high-pressure limit for the total rate coefficient (i.e., including the H abstraction) of OH with ethylene is plotted in Figure 3, along with data reported to be at this limit. Comparisons of the addition rate coefficients obtained with the two-transition-state model with experimental and theoretical values at low temperatures are discussed extensively by Greenwald et al.[56] We find very good agreement between our rate coefficients at the high-pressure limit and the low-temperature experimental data of Vakhtin et al.[16] and the JPL recommendation,[85] as well

as with the measurements of Zellner and Lorenz,[41] Tully[37] and Atkinson et al.[32] at somewhat higher temperatures.

The temperature dependence of the addition rate coefficient is plotted in Figure 4 at several pressures. Because the energy barriers for isomerization are high relative to the reactants, complex **1** is virtually the only one stabilized. As expected of a barrierless addition, this rate coefficient shows a reverse temperature dependence and a strong pressure dependence. The capture rate for OH and ethylene and the stabilization of **1** are discussed in great detail in ref 56. Suffice it to say that the model developed by Greenwald et al.[56] successfully reproduces the available experimental data at low temperatures and predicts negative activation energies in this region.

The total rate coefficients at high temperatures are plotted in Figure 5 along with selected data from experiments and
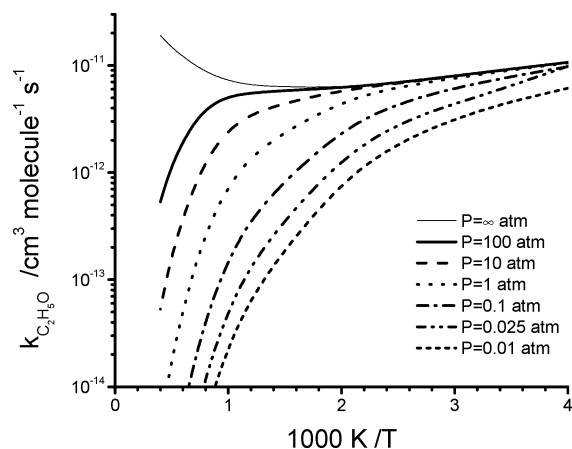
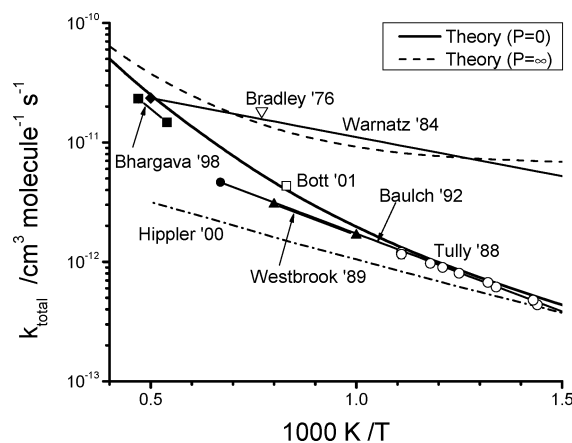**Figure 4.** Arrhenius plot for the addition reaction at several pressures of N_2 diluent.

Figure 5. Arrhenius plot for the total rate coefficient at high temperatures. Experimental data[17,18,45,46,59,60] and data evaluations[87,91] should be near the collisionless limit.
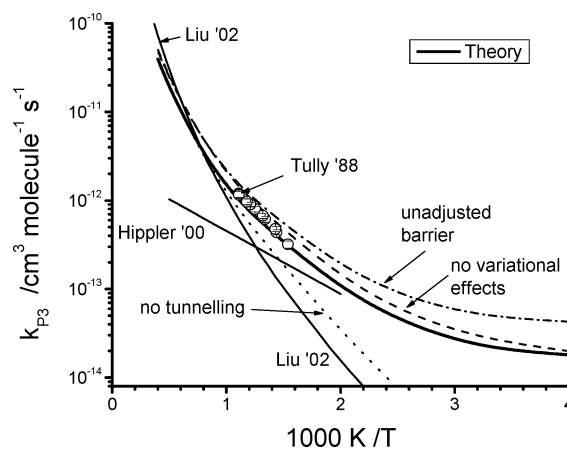

Figure 6. Arrhenius plot for direct hydrogen abstraction (**P3**). Theoretical rate coefficients and the effects of excluding variational and tunneling corrections and adjustments to the barrier from the calculations are shown together with data from other studies.[12,60]
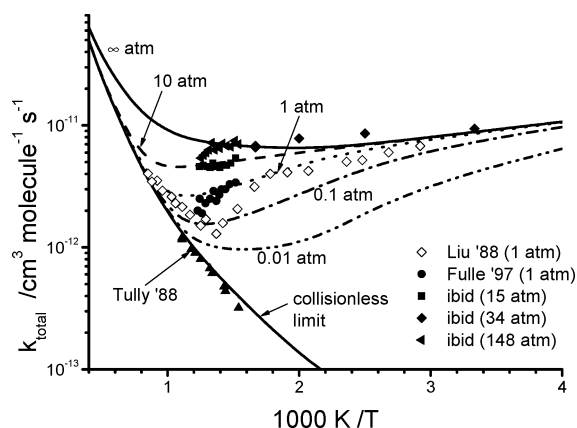

Figure 7. Arrhenius plot for the total reaction of OH with C_2H_4 at several pressures. Also shown are data from Tully at 0.6−0.8 atm He (low[37] and high[45] *T*), Liu et al.[43] at 1 atm of Ar, and Fulle et al.[52] at 1.1 ± 0.1, 15.2 ± 1.3, 34.7 ± 6.2 and 148.2 ± 11.2 atm in He diluent.

evaluations close to the collisionless limit; as well as transition-state theory results from a previous study.[60] Tully[45] used a laser photolysis/laser induced fluorescence technique to measure absolute rate coefficients between 650 and 901 K at about 600 Torr of He. Tully concluded that under these conditions the reaction is dominated by the hydrogen abstraction process. This point was contested in a later study by Hippler and Viskolcz, who calculated a negligible contribution from the hydrogen abstraction channel. This controversy prompted the latest evaluation[86] of kinetic data for combustion modeling to attribute the rate coefficient at high temperatures to channels other than hydrogen abstraction. Our calculations of the collisionless limit confirm the results of Tully's study, although our values are slightly higher at the low-temperature end of his data. Interestingly, calculations using the UB3LYP geometries and frequencies are in excellent agreement with Tully's study.

Given the high precision of Tully's experiments, we decided to adjust the energy barrier by raising the energy of the hydrogen abstraction transition state by 0.4 kcal/mol (150 cm^{-1}). Note that this adjustment is well within the estimated accuracy ($\approx$2 kcal/mol) of the theoretical methods. Rate coefficients at the collisionless limit (after this adjustment) are in good agreement with the shock-tube data from Bott and Cohen[18] and with the upper limit of Warnatz's recommendation. However, the predicted rate coefficients at the collisionless limit are slightly higher ($\approx$30%) than those reported by Bhargava and Westmoreland[59] from flame measurements between 1850 and 2150 K. Our results show somewhat larger activation energies than the

rate coefficients reported by Westbrook et al.[46] and the recommendation of Baulch et al.[87]

Rate coefficients for direct hydrogen abstraction from ethylene by OH radicals are shown in Figure 6. The calculated energy barrier for the hydrogen abstraction reaction is in line with that expected from a simple Evans−Polanyi correlation (the C−H bond dissociation energies of acetylene, ethylene and ethane are 133.6, 111.1 and 100.5 kcal/mol, respectively,[88,89] and the barriers for H abstraction from these molecules are 18.0,[84] 4.9 and 2.5[71] kcal/mol, respectively). This process is pressure independent and is dominant at low pressures and/or high temperatures. Note that in the lower end of the temperature range of Tully's experiments,[45] a nontrivial fraction of the reaction proceeds through the addition reaction or the channel leading to vinyl alcohol, so the calculated rate coefficients for the direct hydrogen abstraction channel (**P3**) are lower than data from ref 45. Also shown in Figure 6 is the effect of neglecting variational and tunneling corrections, as well as the rate coefficients calculated with the unadjusted energy barrier. Below 700 K, the magnitude of the tunneling corrections is the largest of these effects, due to the narrow energy barrier for hydrogen abstraction. However, direct hydrogen abstraction is unimportant at low temperatures (<500 K), even at fairly low pressures.

Theoretically derived rate coefficients for the hydrogen abstraction channel have been reported by Liu et al.[12] and Hippler and Viskolcz;[60] they are also shown in Figure 6. The
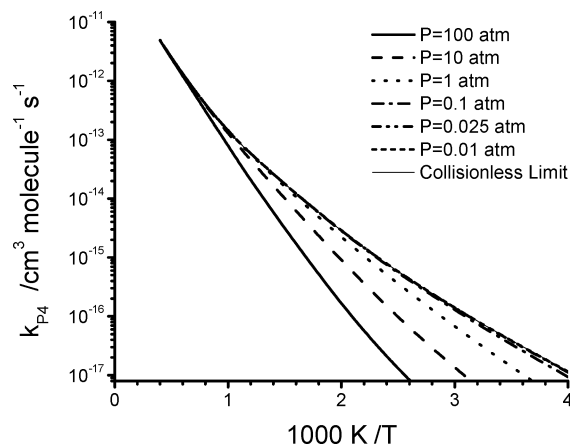
Reaction of Ethylene with Hydroxyl Radicals

J. Phys. Chem. A, Vol. 110, No. 21, 2006 **6967**

Figure 8. Arrhenius plot for the formation of vinoxy alcohol (**P4**) at several pressures of N_2 diluent.
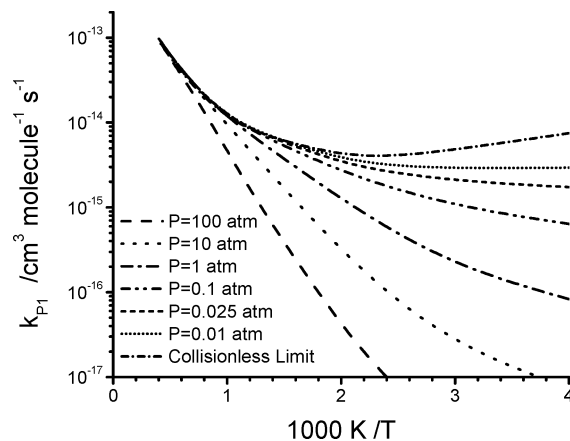
Figure 9. Arrhenius plot for the channel leading to $H_2CO + CH_3$ (**P1**) at several pressures of N_2 diluent.

Figure 10. Arrhenius plot for the channel leading to $CH_3CHO + H$ (**P2**) at several pressures of N_2 diluent.

Figure 11. Product branching fractions at the collisionless limit.

Figure 12. Product branching fractions at 1 atm of N_2 diluent.

calculations of Liu et al. are based on canonical variational transition-state theory with small curvature tunneling (CVT/SCT). Above 650 K, both variational and tunneling corrections reported by this study are quite small (<18%). Rate coefficients from Liu's study are smaller than those from our calculations below 1000 K, and larger above 1500 K. The higher activation energy and larger *A*-factor in ref 12 is probably due to the higher energy barrier and a harmonic treatment of the torsional mode in the transition state used in that study. The study by Hippler and Viskolcz[60] based on transition-state theory concluded that "direct hydrogen abstraction from C_2H_4 is an unimportant process". Their recommended expression is about 2 orders of magnitude lower than our calculations at 1500 K, and it shows a markedly lower activation energy despite the higher energy barrier used in that study.

In calculating variational corrections for the hydrogen abstraction channel, we employed RQCIT//DFT single-point energies and the IRC curve and projected frequencies calculated with the UB3LYP method. The reduction of the rate coefficients of this channel due to variational effects is relatively small (<15%), in agreement with the results of another variational study.[12] Surprisingly, the calculated variational correction factor does not decrease monotonically with increasing temperature. This is due to the loosening of some bending modes with decreasing HO–C_2H_4 separations, and the relatively flat IRC curve after the addition of zero-point energy (i.e., the vibrationally adiabatic potential). The maximum in the RQCIT//DFT adiabatic potential occurs at an $R(C_2H_4$–OH) distance of 1.378 Å, out from the distance of 1.277 Å of the UB3LYP saddlepoint.
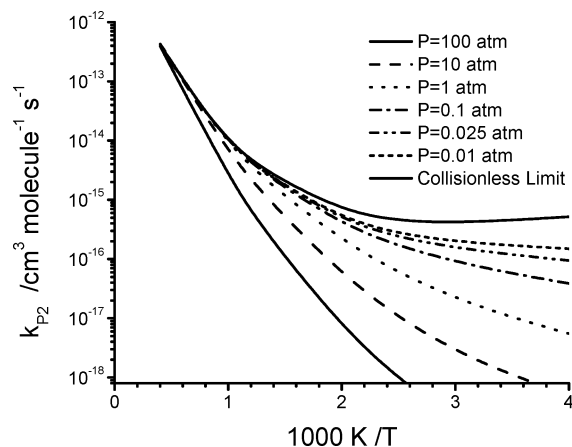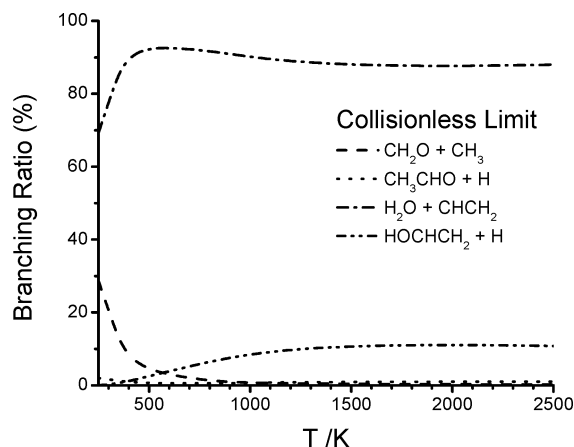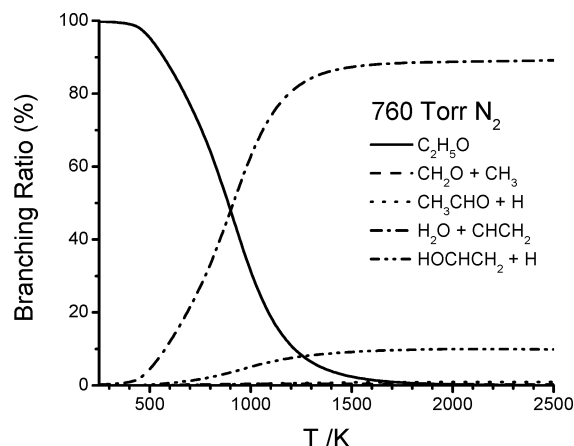
The dynamical transition state moves in from this maximum at very low temperatures (energies), driven by the entropy of the low-frequency modes corresponding to OH rotations. However, at higher temperatures (energies), the lower frequencies of some bending modes increase the entropy of the transition state, bringing the variational correction closer to unity.

Total rate coefficients calculated at several pressures are plotted in Figure 7. The marked change in activation energy reflects a change of the dominant reaction pathway, from the addition channel at temperatures below 600 K to the hydrogen abstraction channel above 1000 K. Liu et al.[44] report rate coefficients in 1 atm of Ar collider between 343 and 1173 K. Although our calculations at 1 atm of N_2 collider gas agree quite

TABLE 6: Fitting Parameters^a for Calculated Rate Coefficients

channel	P (atm)	A	B	C	D	E	F
H$_2$O + CHCH$_2$		2.18×10^{-25}	4.20	−433			
CH$_3$ + CH$_2$O	0	2.65×10^{-25}	3.34	−1397			
	0.01	8.88×10^{-24}	2.92	−872			
	0.025	5.29×10^{-23}	2.71	−590			
	0.1	9.22×10^{-22}	2.36	−91			
	1	2.95×10^{-19}	1.68	1037			
	10	3.94×10^{-15}	0.56	3023			
	100	4.58×10^{-11}	−0.50	5765			
CH$_3$CHO + H	0	1.48×10^{-32}	5.69	−1615			
	0.01	3.94×10^{-31}	5.30	−1032			
	0.025	1.45×10^{-28}	4.57	−311			
	0.1	6.69×10^{-25}	3.54	947			
	1	3.95×10^{-26}	3.91	867			
	10	1.37×10^{-15}	1.01	5288			
	100	1.13×10^{-14}	0.81	6979			
CH$_2$CHOH + H	0	1.68×10^{-20}	2.60	2063			
	0.01	1.72×10^{-20}	2.60	2074			
	0.025	1.78×10^{-20}	2.60	2078			
	0.1	2.53×10^{-20}	2.56	2133			
	1	5.30×10^{-19}	2.19	2645			
	10	3.22×10^{-16}	1.43	3940			
	100	1.42×10^{-13}	0.75	5783			
C$_2$H$_5$O (**1** + **2** + **3**)	0.01	$9.81 \times 10^{+17}$	−10.43	2432	$4.59 \times 10^{+23}$	−11.64	5586
	0.025	$1.00 \times 10^{+14}$	−9.76	1004	$8.23 \times 10^{+13}$	−8.68	2695
	0.1	$1.00 \times 10^{+14}$	−9.65	1189	$4.25 \times 10^{+11}$	−7.79	2525
	1	$1.00 \times 10^{+14}$	−8.14	4048	$1.21 \times 10^{+08}$	−6.91	1437
	10	$1.00 \times 10^{+14}$	−7.77	5403	$5.02 \times 10^{+02}$	−4.87	1156
	100	$1.00 \times 10^{+14}$	−7.44	7181	4.63×10^{-05}	−2.41	509
	∞	$1.00 \times 10^{+14}$	−8.88	2602	7.41×10^{-17}	1.55	−787

^{a} $k(T) = AT^B \exp(-C/T) + DT^E \exp(-F/T)$. Units are cm^3 molecule^{-1} s^{-1} and K.

well with the rate coefficients reported in ref 44 at low and high temperatures, they differ at intermediate temperatures (between 600 and 970 K). Data from Fulle et al.[52] obtained at 1 atm of He are also higher than that of ref 44 in this intermediate region. One possible explanation of this difference is that the thermal redissociation of **1** back to reactants may not have been accounted for properly in the analysis of ref 44. Tully found that redissociation is significant above 500 K, and our calculations show that at 700 K and 1 atm, the rate of association and redissociation of **1** are approximately equal (i.e., $K_{\mathbf{R1}}^{eq}[\text{C}_2\text{H}_4] \approx 1$). Unfortunately, it is not clear if the [OH] time profiles in ref 44 were fit using a single-exponential term.

Vinyl alcohol is formed by H atom elimination from 1-hydroxyethyl radical. This process is competitive with dissociation of this radical to acetaldehyde (through the intermediate complex **2**) despite the slightly higher activation energies due to the larger *A*-factor. Rate coefficients for this reaction are plotted in Figure 8. Our model predicts a nonnegligible amount of vinyl alcohol produced at temperatures above 1200 K. Recently, Taatjes et al.[90] used photoionization mass spectroscopy to identify the presence of enols in low-pressure flames using several fuels. The amount of vinyl alcohol in the experiments of Taatjes et al. was significantly higher than could be expected from enol-ketene tautomerism. Flame calculations based on the present rate coefficients successfully account for the amount of vinyl alcohol observed by Taatjes and co-workers.

A number of species formed as bimolecular products in the reaction of C$_2$H$_4$ with OH have been observed in interstellar clouds, including formaldehyde and vinyl alcohol.[2] In conditions pertaining to interstellar and circumstellar chemistry, formation of formaldehyde and methyl radicals from the decomposition of ethoxy radicals is considerable. Rate coefficients for **P1** are enhanced by high temperatures and low pressures, as can be seen from Figure 9. The rate coefficient for formation of formaldehyde and methyl radicals (**P1**) is limited by the [1,3]-

hydrogen shift. Although the barrier for the [1,3]-hydrogen shift is slightly higher than that of the hydrogen abstraction, tunneling effects are comparatively larger in the former process due to the narrower energy barrier. For instance, the UQCISD/6-311++G(d,p) imaginary frequency for TS(**1**↔**2**) is 2226i cm^{-1}, compared to 1892i cm^{-1} for TS(**R**↔**P3**).

Acetaldehyde and atomic hydrogen (**P2**) are produced by the H atom elimination from ethoxy or 1-hydroxyethyl radicals. The rate-limiting step for this channel is also the isomerization, **1** ↔ **2**. Rate coefficients for acetaldehyde formation also increase at high temperatures and low pressures, as shown in Figure 10. However, other channels (**P1** and **P3**) are favored at these conditions, so the production of acetaldehyde is not important.

Channel switching is the cause of the strong curvature in the Arrhenius plot of the total rate coefficient between ethylene and OH. Product branching ratios as a function of temperature are shown in Figures 11 and 12 for the collisionless limit and for atmospheric pressure, respectively. At low pressures, the hydrogen abstraction channel dominates the reaction over the entire temperature range studied, but at temperatures above 800 K (at atmospheric pressure), the channel leading to vinyl alcohol becomes significant. Above this temperature, the fraction of the vinyl alcohol channel (≈10%) is fairly constant with temperature and pressure.

IV. Concluding Remarks

The present study reports high-level quantum chemistry calculations for all low-energy pathways of the reaction of ethylene with OH radicals. Rate coefficients were computed on the basis of these calculations and the model of Greenwald et al.[56] for the addition channel by means of a multichannel master equation model. Our model reproduces most of the experimental data for the high-pressure rate coefficients available at lower temperatures (below 525 K).

Our calculations confirm the importance of the hydrogen abstraction channel at temperatures above 800 K (at pressures ≤1 atm). With a minor adjustment (0.4 kcal/mol) to the energy barrier of the hydrogen abstraction channel, our calculated rate coefficients in the collisionless limit are in excellent agreement with high-temperature experimental data of recent experiments.[18,45,46,59]

At these high temperatures (above 800 K), a significant fraction of the total reaction leads to vinyl alcohol. Flame calculations[90] based on the present rate coefficients account successfully for the amount of vinyl alcohol recently observed in flames,[90] suggesting that vinyl alcohol should be included in hydrocarbon oxidation models.

Rate coefficients computed at temperatures between 250 and 2500 K were fit to sums of modified Arrhenius expressions. Parameters resulting from these fits are provided in Table 6.

Supporting Information Available: Cartesian coordinates of isomers and saddlepoints optimized at the UQCISD/6-311++G(d,p) level, figures of rotational potentials of internal rotors based on UB3LYP/6-311++G(d,p), and a figure of variational treatment of the hydrogen abstraction channel are available free of charge via the Internet at http://pubs.acs.org.

References and Notes

(1) Moses, J. I.; Lellouch, E.; Bezard, B.; Gladstone, G. R.; Feuchtgruber, H.; Allen, M. *Icarus* **2000**, *145*, 166−202.

(2) Turner, B. E.; Apponi, A. J. *Astrophys. J. Lett.* **2001**, *561*, L207.

(3) Sosa, C.; Schlegel, H. B. *J. Am. Chem. Soc.* **1987**, *109*, 4193−4198.

(4) Sosa, C.; Schlegel, H. B. *J. Am. Chem. Soc.* **1987**, *109*, 7007−7015.

(5) Villà, J.; González-Lafont, A.; Lluch, J. M.; Corchado, J. C.; Espinosa-García, J. *J. Chem. Phys.* **1997**, *107*, 7266−7274.

(6) Sekušak, S.; Liedl, K. R.; Sabljic, A. *J. Phys. Chem. A* **1998**, *102*, 1583−1594.

(7) Caralp, F.; Devolder, P.; Fittschen, C.; Gomez, N.; Hippler, H.; Mereau, R.; Rayez, M. T.; Striebel, F.; Viskolcz, B. *Phys. Chem. Chem. Phys.* **1999**, *1*, 2935−2944.

(8) Hoyermann, K.; Olzmann, M.; Seeba, J.; Viskolcz, B. *J. Phys. Chem. A* **1999**, *103*, 5692−5698.

(9) Yamada, T.; Bozzelli, J. W.; Lay, T. *J. Phys. Chem. A* **1999**, *103*, 7646−7655.

(10) Álvarez-Idaboy, J. R.; Mora-Diez, N.; Vivier-Bunge, A. *J. Am. Chem. Soc.* **2000**, *122*, 3715−3720.

(11) Piqueras, M. C.; Crespo, R.; Nebot-Gil, I.; Tomas, F. *Theochem* **2001**, *537*, 199−212.

(12) Liu, G. X.; Ding, Y. H.; Li, Z. S.; Fu, Q.; Huang, X. R.; Sun, C. C.; Tang, A. C. *Phys. Chem. Chem. Phys.* **2002**, *4*, 1021−1027.

(13) Zhang, Y.; Zhang, S. W.; Li, Q. S. *Chem. Phys.* **2004**, *296*, 79−86.

(14) Senosiain, J. P.; Miller, J. A.; Klippenstein, S. J. *Joint Meeting of the U. S. Sections of the Combustion* Institute, 2005.

(15) Zhang, Y.; Zhang, S. W.; Li, Q. S. *Chem. Phys.* **2005**, *308*, 109−116.

(16) Vakhtin, A. B.; Murphy, J. E.; Leone, S. R. *J. Phys. Chem. A* **2003**, *107*, 10055−10062.

(17) Bradley, J. N.; Capey, W. D.; Fair, R. W.; Pritchard, D. K. *Int. J. Chem. Kinet.* **1976**, *8*, 549−561.

(18) Bott, J. F.; Cohen, N. *Int. J. Chem. Kinet.* **1991**, *23*, 1075−1094.

(19) Frenklach, M.; Wang, H.; Rabinowitz, M. J. *Prog. Energy Combust. Sci.* **1992**, *18*, 47−73.

(20) Hidaka, Y.; Nishimori, T.; Sato, K.; Henmi, Y.; Okuda, R.; Inami, K.; Higashihara, T. *Combust. Flame* **1999**, *117*, 755−776.

(21) Bradley, J. N.; Hack, W.; Hoyerman, K.; Wagner, H. G. *J. Chem. Soc., Faraday Trans. 1* **1973**, *69*, 1889−1898.

(22) Greiner, N. R. *J. Chem. Phys.* **1970**, *53*, 1284−1285.

(23) Morris, E. D.; Stedman, D. H.; Niki, H. *J. Am. Chem. Soc.* **1971**, *93*, 3570−3572.

(24) Davis, D. D.; Huie, R. E.; Herron, J. T. *J. Chem. Phys.* **1973**, *59*, 628−634.

(25) Smith, I. W. M.; Zellner, R. *J. Chem. Soc., Faraday Trans. 2* **1973**, *69*, 1617−1627.

(26) Gordon, S.; Mulac, W. A. *Proc. Symp. Chem. Kinet. Data Upper Lower Atmos.* **1974**, 289.

(27) Atkinson, R.; Pitts, J. N. *J. Chem. Phys.* **1975**, *63*, 3591−3595.

(28) Davis, D. D.; Fischer, S.; Schiff, R.; Watson, R. T.; Bollinger, W. *J. Chem. Phys.* **1975**, *63*, 1707−1712.

(29) Pastrana, A. V.; Carr, R. W. *J. Phys. Chem.* **1975**, *79*, 765−770.

(30) Howard, C. J. *J. Chem. Phys.* **1976**, *65*, 4771−4777.

(31) Lloyd, A. C.; Darnall, K. R.; Winer, A. M.; Pitts, J. N. *J. Phys. Chem.* **1976**, *80*, 789−794.

(32) Atkinson, R.; Perry, R. A.; Pitts, J. N. *J. Chem. Phys.* **1977**, *66*, 1197−1201.

(33) Atkinson, R.; Perry, R. A.; Pitts, J. N. *J. Chem. Phys.* **1977**, *67*, 3170−3174.

(34) Overend, R.; Paraskevopoulos, G. *J. Chem. Phys.* **1977**, *67*, 674−679.

(35) Farquharson, G. K.; Smith, R. H. *Aust. J. Chem.* **1980**, *33*, 1425−1435.

(36) Atkinson, R.; Aschmann, S. M.; Winer, A. M.; Pitts, J. N. *Int. J. Chem. Kinet.* **1982**, *14*, 507−516.

(37) Tully, F. P. *Chem. Phys. Lett.* **1983**, *96*, 148−153.

(38) Atkinson, R.; Aschmann, S. M. *Int. J. Chem. Kinet.* **1984**, *16*, 1175−1186.

(39) Klein, T.; Barnes, I.; Becker, K. H.; Fink, E. H.; Zabel, F. *J. Phys. Chem.* **1984**, *88*, 5020−5025.

(40) Schmidt, V.; Zhu, G. Y.; Becker, K. H.; Fink, E. H. *Ber. Bunsen-Ges. Phys. Chem.* **1984**, *89*, 321−322.

(41) Zellner, R.; Lorenz, K. *J. Phys. Chem.* **1984**, *88*, 984−989.

(42) Atkinson, R. *Chem. Rev.* **1986**, *86*, 69−201.

(43) Liu, A.; Mulac, W. A.; Jonah, C. D. *Int. J. Chem. Kinet.* **1987**, *19*, 25.

(44) Liu, A. D.; Mulac, W. A.; Jonah, C. D. *J. Phys. Chem.* **1988**, *92*, 3828−3833.

(45) Tully, F. P. *Chem. Phys. Lett.* **1988**, *143*, 510−514.

(46) Westbrook, C. K.; Thornton, M. M.; Pitz, W. J.; Malte, P. C. *Proc. Combust. Inst.* **1989**, *22*, 863.

(47) Nielsen, O. J.; Jorgensen, O.; Donlon, M.; Sidebottom, H. W.; O'Farrell, D. J.; Treacy, J. *Chem. Phys. Lett.* **1990**, *168*, 319−323.

(48) Becker, K. H.; Geiger, H.; Wiesen, P. *Chem. Phys. Lett.* **1991**, *184*, 256−261.

(49) Diau, E.; Lee, Y. P. *J. Chem. Phys.* **1991**, *96*, 377.

(50) Kuo, C. H.; Lee, Y. P. *J. Phys. Chem.* **1991**, *95*, 1253−1257.

(51) Diau, E. W. G.; Lee, Y. P. *J. Chem. Phys.* **1992**, *96*, 377−386.

(52) Fulle, D.; Hamann, H. F.; Hippler, H.; Jansch, C. P. *Ber. Bunsen.-Ges. Phys. Chem.* **1997**, *101*, 1433−1442.

(53) Chuong, B.; Stevens, P. S. *J. Phys. Chem. A* **2000**, *104*, 5230−5237.

(54) Singleton, D. L.; Cvetanovic, R. J. *J. Am. Chem. Soc.* **1976**, *98*, 6812−6819.

(55) Smith, I. W. M.; Ravishankara, A. R. *J. Phys. Chem. A* **2002**, *106*, 4798−4807.

(56) Greenwald, E. E.; North, S. W.; Georgievskii, Y.; Klippenstein, S. J. *J. Phys. Chem. A* **2005**, *109*, 6031−6044.

(57) Georgievskii, Y.; Klippenstein, S. J. *J. Chem. Phys.* **2005**, *122*, 194103; 1−17.

(58) Zhu, R. S.; Park, J.; Lin, M. C. *Chem. Phys. Lett.* **2005**, *408*, 25−30.

(59) Bhargava, A.; Westmoreland, P. R. *Combust. Flame* **1998**, *113*, 333−347.

(60) Hippler, H.; Viskolcz, B. *Phys. Chem. Chem. Phys.* **2000**, *2*, 3591−3596.

(61) Becke, A. *Phys. Rev. A* **1988**, *38*, 3098−3100.

(62) Stephens, P. J.; Devlin, F. J.; Chabalowski, C. F.; Frisch, M. J. *J. Phys. Chem.* **1994**, *98*, 11623−11627.

(63) Martin, J. M. L. *Chem. Phys. Lett.* **1996**, *259*, 669−678.

(64) Feller, D.; Dixon, D. A. *J. Chem. Phys.* **2001**, *115*, 3484−3496.

(65) Mayer, P. M.; Parkinson, C. J.; Smith, D. M.; Radom, L. *J. Chem. Phys.* **1998**, *108*, 604−615.

(66) Senosiain, J. P.; Klippenstein, S. J.; Miller, J. A. Manuscript in preparation.

(67) Lynch, B. J.; Fast, P. L.; Harris, M.; Truhlar, D. G. *J. Phys. Chem. A* **2000**, *104*, 4811−4815.

(68) Werner, H.-J.; Knowles, P. J.; Amös, R. D.; Bernhardsson, A.; Berning, A.; Celani, P.; Cooper, D. L.; Deegan, M. J. O.; Doobbyn, A. J.; Eckert, F.; Hampel, C.; Hetzer, G.; Korona, T.; Lindh, R.; Lloyd, A. W.; McNicholas, S. J.; Manby, F. R.; Meyer, W.; Mura, M. E.; Nicklass, A.; Palmieri, P.; Pitzer, R.; Rauhut, G.; Schütz, M.; Schumann, U.; Stroll, H.; Stone, A. J.; Tarroni, R.; Thorsteinsson, T. MOLPRO is a package of ab initio programs ver. version 2002.1, 1998.

(69) Frisch, M. J.; Trucks, G. W.; Schlegel, H. B.; Scuseria, G. E.; Robb, M. A.; Cheeseman, J. R.; Zakrzewski, V. G.; Montgomery, J.; Stratmann, R. E.; Burant, J. C.; Dapprich, S.; Millam, J. M.; Daniels, A. D.; Kudin, K. N.; Strain, M. C.; Farkas, O.; Tomasi, J.; Barone, V.; Cossi, M.; Cammi, R.; Mennucci, B.; Pomelli, C.; Adamo, C.; Clifford, S.; Ochterski, J.; Petersson, G. A.; Ayala, P. Y.; Cui, Q.; Morokuma, K.; Malick, D. K.; Rabuck, A. D.; Raghavachari, K.; Foresman, J. B.; Cioslowski, J.; Ortiz, J. V.; Baboul, A. G.; Stefanov, B. B.; Liu, G.; Liashenko, A.; Piskorz, P.; Komaromi, I.; Gomperts, R.; Martin, R. L.; Fox, D. J.; Keith, T.; Al-Laham, M. A.; Peng, C. Y.; Nanayakkara, A.; Challacombe, M.; Gill, P. M. W.; Johnson, B.; Chen, W.; Wong, M. W.; Andres, J. L.; González, C.; Head-Gordon, M.; Replogle, E. S.; Pople, J. A. *Gaussian 98*, revision A.7; Gaussian, Inc.: Pittsburgh, PA, 1998.

(70) Pitzer, K. S.; Gwinn, W. D. *J. Chem. Phys.* **1942**, *10*, 428−440.

(71) Senosiain, J. P.; Musgrave, C. B.; Golden, D. M. *J. Phys. Chem. A* **2001**, *105*, 1669−1675.

(72) Poling, B. E.; Prausnitz, J. M.; O'Connell, J. P. *The Properties of Gases and Liquids*, 5th ed.; McGraw-Hill: New York, 2001.

(73) Miller, J. A.; Klippenstein, S. J.; Robertson, S. H. *J. Phys. Chem. A* **2000**, *104*, 7525−7536. See also: *J. Phys. Chem. A* **2000**, *104*, 9806−9806 (correction).

(74) Klippenstein, S. J.; Miller, J. A. *J. Phys. Chem. A* **2002**, *106*, 9267−9277.

(75) Miller, J. A.; Klippenstein, S. J. *J. Phys. Chem. A* **2003**, *107*, 2680−2692.

(76) Klippenstein, S. J.; Wagner, A. F.; Dunbar, R. C.; Wardlaw, D. M.; Robertson, S. H.; Miller, J. A. VARIFLEX ver. 1.13m, 2003.

(77) Miller, J. A.; Parrish, C.; Brown, N. J. *J. Phys. Chem.* **1986**, *90*, 3339−3345.

(78) Hahn, D. K.; Klippenstein, S. J.; Miller, J. A. *Faraday Discuss.* **2001**, *119*, 79−100.

(79) NIST. Standard Reference Database, Chemistry Webbook. 2003; http://webbook.nist.gov/chemistry/.

(80) Scott, A. P.; Radom, L. *J. Phys. Chem.* **1996**, *100*, 16502−16513.

(81) Wong, M. W. *Chem. Phys. Lett.* **1996**, *256*, 391−399.

(82) Lee, T. J.; Taylor, P. R. *International Symposium on Quantum Chemistry, Solid-State Theory and Molecular Dynamics*; 1989; Vol. 23, pp 199−207.

(83) Lee, T. J.; Rendell, A. P.; Taylor, P. R. *J. Phys. Chem.* **1990**, *94*, 5463−5468.

(84) Senosiain, J. P.; Miller, J. A.; Klippenstein, S. J. *J. Phys. Chem. A* **2005**, *109*, 6045−6055.

(85) DeMore, W. B.; Sander, S. P.; Golden, D. M.; Hampson, R. F.; Kurylo, M. J.; Howard, C. J.; Ravishankara, A. R.; Kolb, C. E.; Molina, M. J. Chemical Kinetics and Photochemical Data for use in Stratospheric Modeling. NASA-JPL, 1997.

(86) Baulch, D. L.; Bowman, C. T.; Cobos, C. J.; Cox, R. A.; Just, T.; Kerr, J. A.; Pilling, M. J.; Stocker, D.; Troe, J.; Tsang, W.; Walker, R. W.; Warnatz, J. *J. Phys. Chem. Ref. Data* **2005**, *34*, 757−1397.

(87) Baulch, D. L.; Cobos, C. J.; Cox, R. A.; Esser, C.; Frank, P.; Just, T.; Kerr, J. A.; Pilling, M. J.; Troe, J.; Walker, R. W.; Warnatz, J. *J. Phys. Chem. Ref. Data* **1992**, *21*, 411−734.

(88) Tsang, W. Heats of Formation of Organic Free Radicals by Kinetic Methods. In *Energetics of Organic Free Radicals*; Simões, J. A. M., Ed.; Blackie Academic and Professional: London, 1996; p 22.

(89) Senosiain, J.; Han, J.; Musgrave, C.; Golden, D. *Faraday Discuss.* **2001**, *119*, 173−189.

(90) Taatjes, C. A.; Hansen, N.; McIlroy, A.; Miller, J. A.; Senosiain, J. P.; Klippenstein, S. J.; Qi, F.; Sheng, L.; Zhang, Y.; Cool, T. A.; Wang, J.; Westmoreland, P. R.; Law, M. E.; Kasper, T.; Kohse-Höinghaus, K. *Science* **2005**, *308*, 1887−1889.

(91) Warnatz, J. Rate coefficients in the C/H/O system. *Combustion Chemistry*; 1984; p 197.

(92) IRCmax is the maximum energy barrier calculated at a high level of theory (i.e., RQCISD(T)/cc-pV∞Z) using geometries optimized along the IRC curve calculated with a lower level of theory (i.e., UB3LYP/6-311++G(d,p)). (See Malick, D. K.; Petersson, G. A.; Montgomery, J. A. *J. Chem. Phys.* **1998**, *108*, 5704−5713.)